Gain-scheduling LPV control for autonomous vehicles including friction force estimation and compensation mechanism

Eugenio Alcala ✉, Vicenç Puig, Joseba Quevedo, Teresa Escobet

Research Center of Supervision, Safety and Automatic Control (CS2AC), Advanced Control Systems Group, Universitat Politècnica de Catalunya (UPC), Rambla Sant Nebridi, 10, 08222 Terrassa, Spain

✉ *E-mail: eugenio.alcala@upc.edu*

Abstract: This study presents a solution for the integrated longitudinal and lateral control problem of urban autonomous vehicles. It is based on a gain-scheduling linear parameter-varying (LPV) control approach combined with the use of an Unknown Input Observer (UIO) for estimating the vehicle states and friction force. Two gain-scheduling LPV controllers are used in cascade configuration that use the kinematic and dynamic vehicle models and the friction and observed states provided by the Unknown Input Observer (UIO). The LPV–UIO is designed in an optimal manner by solving a set of linear matrix inequalities (LMIs). On the other hand, the design of the kinematic and dynamic controllers lead to solve separately two LPV–Linear Quadratic Regulator problems formulated also in LMI form. The UIO allows to improve the control response in disturbance affected scenarios by estimating and compensating the friction force. The proposed scheme has been integrated with a trajectory generation module and tested in a simulated scenario. A comparative study is also presented considering the cases that the friction force estimation is used or not to show its usefulness.

1 Introduction

The European Parliament Research Service considers autonomous driving as one of the top ten technologies that will change citizen's life the most [1]. This comes with no surprise given the clear benefits that one can foresee, in particular: (i) achievement of almost zero traffic accidents by taking humans out of the driving task; (ii) inclusion of citizens with low physical mobility by the introduction of door-to-door transportation services; (iii) reduction of congestion by route sharing (passengers and goods) and a centralised mobility intelligence; (iv) decrease of energy consumption and pollution by relying on electric vehicles with a smarter vehicle control.

Recently, industrialised countries carry out a technological race toward autonomous driving. Research institutions and powerful companies of the automotive, mobility and software sectors are accelerating their achievements by a great investment in human and technology resources. In spite of the gigantic difficulties of reaching full autonomy at all times and in all the places, the recent advances in hardware (sensors, embedded super-computers etc.), software (artificial intelligence, planning and control, telecommunications etc.), laws and potential user acceptance seem to indicate that reaching autonomous driving is just a matter of time.

Nowadays, half the world's population live in cities, and the World Health Organization predicts that by 2050 this proportion will increase to 66% [2], straining city traffic more and more. City scenarios, then, are of high relevance and present routes, speeds, traffic signs, infrastructure elements and surroundings that are much more difficult to understand than on highways or segregated lanes, not to mention the need to take care of pedestrians and cyclists.

Overall, the process will be an incremental approach, with a long period of coexistence between human and artificial drivers. For that purpose, the Society of Automotive Engineers (SAE) defines five progressive levels of automation [3], from driver assistance (Level 1) to full automation (Level 5), which are not expected before 2025. From Level 2 to Level 5, the vehicle takes full control of the accelerating, braking and steering tasks. This means that an automatic control software will tackle the velocity and position control while handling a suitable dynamic behaviour.

Automatic control is one of the most important tasks within the autonomous driving system [4]. The control objective is to follow the references provided by the trajectory generator This is a complex task that must guarantee the vehicle stability as well as ensure certain levels of performance. Moreover, in addition to implement control algorithm, this automatic control module has to deal with real data management through sensors and actuators. In particular, first, it is required to measure vehicle variables and understand the environment located around the vehicle using sensors (global positioning system, inertial measurement unit, encoders, cameras, light detection and ranging etc). Then, commanding proper signals to actuators (steering motor, electric engine and brake system) to perform the motion of the vehicle following the pre-established trajectory. Recently, the energy management has also begun to be considered as an additional aspect to address when solving the control problem of autonomous vehicles. See, as, e.g. [5], where an optimal speed control strategy is proposed to minimise accelerations taking into account traffic signals, speed limits and previous vehicle information.

The problem of trajectory tracking control is usually defined by three general aspects: the type of control (lateral, longitudinal or both), the type of the model considered (kinematic, linear dynamic, non-linear simplified dynamic or non-linear dynamic) and the control strategy to be used. Until now, different tracking control problems have been treated such as the longitudinal control, the lateral control and the mixed one that includes both cases. The goal in the longitudinal control task is to maintain the linear velocity of the vehicle around a given velocity set point while performing with smooth accelerations. This is known as cruise control. At this point, the driver is released of the accelerating and braking tasks, being the autonomous system responsibility. This case is included in the Level 1 of automation defined by the SAE [3] and an example of this control problem is shown in [6]. On the other hand, the lateral control is in charge of controlling the yaw movement of the vehicle. To do so, the controller acts over the angle of the front wheels. This case is the opposite one of the longitudinal control task. In this case, the driver only controls the acceleration and brakes, being the automatic controller in charge of turning. In [7], a good example of this control case is presented. The last control problem is the mixed one. In this case, the automatic control module governs the complete two-dimensional vehicle motion, i.e.

Table 1 Classification of control techniques according to the type of model

	Mixed control problem	
Control strategy	Kinematic model	Dynamic model
H_∞	[9]	
SMC–SMC adaptive	[10]	
Lyapunov	[10–13]	
LPV	[8]	[14, 15]
T–S	[12]	
MPC	[16, 17]	[16, 18]
non-linear MPC	[19, 20]	[21–23]

full control of the accelerating, braking and steering tasks and rises to the levels 2–5 of automation, for instance in [8].

To address these control problems, several types of vehicle models are considered. On one hand, kinematic models are a function of vehicle geometry. On the other hand, dynamic ones rely on physical models to describe the interaction between the vehicle and the road. Section 2 goes in deep in this topic.

The third aspect that defines the autonomous guidance problem is the choice of the control strategy. This selection is often being related with the selection of the vehicle model, i.e. a linear model will require a linear technique, whereas a non-linear one will involve a non-linear strategy. So far, several control strategies have been proposed each one with different advantages to the application to the autonomous guidance problem. Some of the most relevant strategies in the autonomous driving field according to Paden *et al.* [4] are: proportional–integral–derivative (PID), H_∞, fuzzy logic control, sliding mode control (SMC), Lyapunov-based control, linear parameter varying (LPV), Takagi–Sugeno (T–S), linear quadratic regulator (LQR) and model predictive control (MPC), see Table 1.

The real autonomous guidance situation involves addressing the mixed control problem that requires solving the longitudinal and lateral vehicle control problem at the same time, being this the target of this paper. A classification of the different control strategies dealing with the mixed control problem according to the type of model has been presented in Table 1 with the corresponding references.

Some of the previously enumerated control strategies (such as PID, fuzzy logic control or LQR) do not appear in the table due to they mostly have been applied to solve the lateral control problem.

The LPV technique has proven to be an advanced control strategy in recent years. This allows solving non-linear problems using a pseudo-linear model by embedding the non-linearities inside model parameters that depend on some scheduling variables. Recent books, [15, 24–26], present the study of LPV modelling and design under the linear matrix inequality (LMI)-based formulation. Several design approaches can be used as pole placement, H_∞, H_2 and optimal methods.

The lack of measurement of certain vehicle states as well as the ignorance of external disturbances can generate a problem when applying the previously designed control to follow the proposed path. The measurement of states will depend on the type of sensors installed on the vehicle and is vital for the application of certain types of control such as state feedback. Longitudinal velocity and yaw rate are easily measured using low cost sensors that are actually installed on many of existing vehicles. However, other states, which have also a huge impact on vehicle dynamics, are more difficult to measure using vehicle sensors. For example, this is the case of the slip angle.

The friction forces are one of the most significant disturbances that affect a vehicle. This force is dependent on the type of materials involved in the wheel–road contact. The most common, rubber-asphalt, generates a magnitude of friction force that can be drastically altered if the vehicle suddenly crosses a wet or even frozen area. For this reason, the estimation and subsequent compensation by the control strategy of this force is of great interest in the field of autonomous driving.

Several approaches have been recently studied in the state-disturbance estimation area for autonomous vehicles including observer-based [27, 28] and statistical [29] methods. One of the observer-based technique is the UIO. This technique has been widely used for fault detection and isolation as, e.g. in [30]. These type of observers allow to estimate the states of a system as well as disturbances or unmodelled uncertainty in the system. However, the application of UIOs to the case of vehicle friction force estimation has not been presented yet.

This paper presents a solution for the integrated longitudinal and lateral control problem of urban autonomous vehicles. This solution is based on a gain-scheduling LPV control approach combined with the use of an UIO for estimating the vehicle states and friction force. The contribution of this article is three-fold. First, we present a novel LMI formulation for the LPV–UIO observer design based on an optimal approach. It follows the control–observer duality principle and introduces also a constraint for the decay rate. Second, a friction force compensation mechanism based on the estimation provided LPV–UIO is proposed for reducing the control effort and increasing the response when such a disturbance actuates. Third, we present the design of an LPV–LQR approach for solving the integrated lateral and longitudinal control for autonomous vehicles. This approach is based on a cascade design of the kinematic and dynamic controllers. Such a cascade scheme is based on the idea that the dynamic closed-loop behaviour is designed to be faster than the kinematic closed-loop one.

The proposed scheme is integrated with a trajectory generation module and tested in a simulated scenario. A comparative study is also presented considering the cases that the friction force estimation is used or not to show its usefulness.

This paper is structured as follows: Section 2 presents and describes the different types of vehicle models used for control and estimation purposes. In Section 3, the LPV modelling is developed. Section 4 shows the UIO design using the gain-scheduling LPV approach. Section 5 presents the feedback control design. Finally, Section 6 shows the results and Section 7 presents the conclusions of the work.

2 Kinematic and dynamic vehicle models

This section describes the models which will be used later for developing the automatic control strategies. A mobile object can be described by using equations that represent the dynamic and kinematic behaviours. Unlike common mobile robots, urban autonomous vehicles are systems with larger mass and operating at a higher velocity. Hence, the use of dynamic models becomes indispensable. On one hand, in dynamic models the sum of forces existing over the vehicle is taken into account for computing the vehicle acceleration. The motion is generated by applying forces over the driven wheels and mass, inertial and tyre parameters are considered. On the other hand, kinematic model is based on the velocity vector movement in order to compute longitudinal and lateral velocities referenced to a global inertial frame. External forces are not considered in this case. Note that, for both models, the two wheels bicycle model has been considered as the one depicted in Fig. 1. It is interesting to specify that the two wheels model employed does not consider *roll*, *pitch* and z motion, only *yaw*, x and y movements.

In this work, both models are presented and used in a decoupled way. It means that both model behaviours will be controlled in a decoupled way by using a cascade control scheme. Table 2 presents the characteristic vehicle parameters used in the models.

2.1 Kinematic model

Kinematic-based model is widely used due to its low parameter dependency. It assumes null skidding and considers lateral force to be so small that can be neglected. Basically, it is a geometric manner to compute vehicle position and orientation considering linear and angular velocities. The kinematic equations are

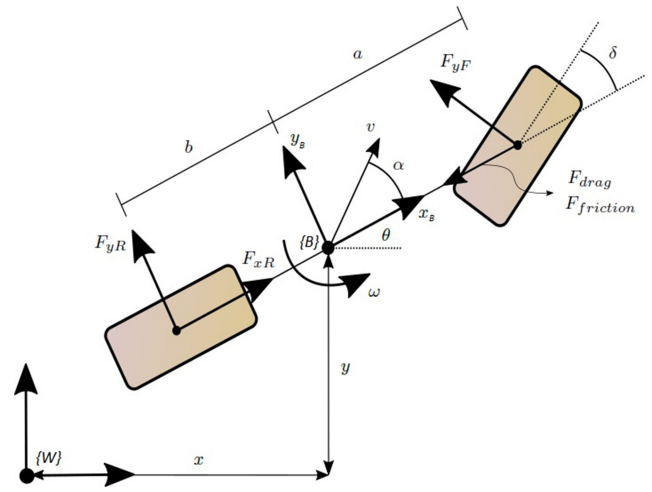

Fig. 1 *Two wheels bicycle model used for control purposes. {W} frame represents the global inertial frame and {B} is the body frame located in the centre of gravity of the vehicle*

Table 2 Kinematic and dynamic model parameters

Parameter	Description	Value
a	distance from CoG to front axle	0.758 m
b	distance from CoG to rear axle	1.036 m
M	vehicle mass	683 kg
I	vehicle yaw inertia	560.94 kg m^2
C_d	drag coefficient	0.36
A_r	vehicle frontal area	1.91 m^2
ρ	air density at 25°C	1.184 $\frac{\text{kg}}{\text{m}^3}$
μ_o	nominal friction coefficient	0.5
C_x	tyre stiffness coefficient	25,000 $\frac{N}{\text{rad}}$

CoG means Center of Gravity.

$$\begin{cases} \dot{x} = v\cos(\theta) \\ \dot{y} = v\sin(\theta) \\ \dot{\theta} = \omega \end{cases} \tag{1}$$

where x, y and θ represent the current position and orientation of the vehicle in metres (m) and radians (rad), respectively, with respect to the inertial frame $\{W\}$. v is the linear velocity measured in (m/s) and ω represents the vehicle angular velocity in (rad/s).

2.2 Dynamic model

The dynamical behaviour of a vehicle is generally complicated to represent in a detailed manner. In practical applications, normally simplified models are used. In this case, the obtained model is based on the second Newton's law. The streamlined dynamical model of the road vehicle can be written as

$$\begin{aligned} \dot{v} &= \frac{F_{x\mathrm{R}}\cos(\alpha) + F_{y\mathrm{F}}\sin(\alpha-\delta) + F_{y\mathrm{R}}\sin(\alpha) - F_{df}}{M} \\ \dot{\alpha} &= \frac{-F_{x\mathrm{R}}\sin(\alpha) + F_{y\mathrm{F}}\cos(\alpha-\delta) + F_{y\mathrm{R}}\cos(\alpha)}{Mv} - \omega \\ \dot{\omega} &= \frac{F_{y\mathrm{F}}a\cos(\delta) - F_{y\mathrm{R}}b}{I} \end{aligned} \tag{2}$$

$$F_{y\mathrm{F}} = C_x\left(\delta - \alpha - \frac{a\omega}{v}\right) \tag{3}$$

$$F_{y\mathrm{R}} = C_x\left(-\alpha + \frac{b\omega}{v}\right) \tag{4}$$

$$F_{df} = F_{\mathrm{drag}} + F_{\mathrm{friction}} = \frac{1}{2}C_{\mathrm{d}}\rho A_{\mathrm{r}}v^2 + \mu_{\mathrm{o}}Mg \tag{5}$$

where α represents the vehicle slip angle (rad), δ is the steering angle and one of the inputs of the system (rad), $F_{x\mathrm{R}}$ is the longitudinal rear force and the other input of the system (N), $F_{y\mathrm{R}}$ represents the lateral rear force that appears when steering (N), $F_{y\mathrm{F}}$ is the lateral front force which appears also with the angular motion (N), F_{drag} represents drag force that opposes to the forward movement (N) and F_{friction} is the friction force that also opposes to the longitudinal vehicle movement (N). Note that μ_{o} represents a nominal value for the friction coefficient. In addition, note that instead of employing the states x and y, a new representation has been adopted by using the polar representation and considers the variables v and α. These variables can be seen in Fig. 1. Observe that the dynamic model variables are referred to the vehicle body frame $\{B\}$ whereas the kinematic set of variables refers to the global fixed coordinate system $\{W\}$ in order to represent the trajectory from a relative point of view.

3 LPV control-oriented model

The LPV control technique requires a linear-like representation of the non-linear model to be controlled. Hence, the LPV modelling task is presented in this section. This method consists on embedding the non-linearities inside model parameters that depend on some variables, called scheduling variables, that vary in a known bounded interval. In the last section, kinematic and dynamic non-linear models were presented. Here, an LPV representation for each one is introduced. For the kinematic LPV modelling task, a reference model has been built previously. Note that two decoupled LPV models have been obtained in order to control the kinematic and dynamic parts of the vehicle separately.

3.1 Kinematic LPV modelling

To obtain the kinematic LPV model, a reference model has been developed. This model is defined as the difference between real measurements (x, y and θ) and desired values ($x_{\mathrm{d}}, y_{\mathrm{d}}$ and θ_{d}). However, these set of errors are expressed with respect to the inertial global frame $\{W\}$ (see Fig. 1). For control purposes is suitable to express the errors with respect to the vehicle, such that the lateral error is always measured in the lateral axis of the vehicle. Thus, a rotation over the road orthogonal axis is considered to represent the errors in the body vehicle frame $\{B\}$

$$\begin{bmatrix} x_{\mathrm{e}} \\ y_{\mathrm{e}} \\ \theta_{\mathrm{e}} \end{bmatrix} = \begin{bmatrix} \cos(\theta) & \sin(\theta) & 0 \\ -\sin(\theta) & \cos(\theta) & 0 \\ 0 & 0 & 1 \end{bmatrix} \begin{bmatrix} x_{\mathrm{d}} - x \\ y_{\mathrm{d}} - y \\ \theta_{\mathrm{d}} - \theta \end{bmatrix} \tag{6}$$

where subindexes d and e represent the desired and error values, respectively. To obtain the error model it is necessary to take into account the rear wheels non-holonomic constraint of the form

$$\dot{x}\sin(\theta) = \dot{y}\cos(\theta)\,. \tag{7}$$

Hence, computing the time derivative of (6) and using (1), (7) plus some trigonometric identity, we obtain the following open-loop error system:

$$\begin{aligned} \dot{x}_{\mathrm{e}} &= \omega y_{\mathrm{e}} + v_{\mathrm{d}}\cos\theta_{\mathrm{e}} - v \\ \dot{y}_{\mathrm{e}} &= -\omega x_{\mathrm{e}} + v_{\mathrm{d}}\sin\theta_{\mathrm{e}} \\ \dot{\theta}_{\mathrm{e}} &= \omega_{\mathrm{d}} - \omega\,. \end{aligned} \tag{8}$$

Details about the development of (8) can be found in Chapter 1 of [13]. At this point, denoting the state, control and output vectors, respectively, as

$$\boldsymbol{x}_{\mathrm{C}} = \begin{bmatrix} x_{\mathrm{e}} \\ y_{\mathrm{e}} \\ \theta_{\mathrm{e}} \end{bmatrix}, \quad \boldsymbol{u}_{\mathrm{C}} = \begin{bmatrix} v \\ \omega \end{bmatrix}, \quad \boldsymbol{r}_{\mathrm{C}} = \begin{bmatrix} v_{\mathrm{d}} \cos\theta_e \\ \omega_{\mathrm{d}} \end{bmatrix} \tag{9}$$

we can obtain the LPV representation for the kinematic dynamics (8). Then, considering ω, v_{d}, $\theta_{\mathrm{e}} \in \mathbb{R}$ as the kinematic scheduling variables, the LPV form becomes

$$\dot{\boldsymbol{x}}_{\mathrm{C}} = \boldsymbol{A}_{\mathrm{C}}(\omega, v_{\mathrm{d}}, \theta_{\mathrm{e}})\boldsymbol{x}_{\mathrm{C}} + \boldsymbol{B}_{\mathrm{C}}\boldsymbol{u}_{\mathrm{C}} - \boldsymbol{B}_{\mathrm{C}}\boldsymbol{r}_{\mathrm{C}} \tag{10a}$$

where

$$\boldsymbol{A}_{\mathrm{C}}(\omega, v_{\mathrm{d}}, \theta_{\mathrm{e}}) = \begin{bmatrix} 0 & \omega & 0 \\ -\omega & 0 & v_{\mathrm{d}}\dfrac{\sin\theta_{\mathrm{e}}}{\theta_{\mathrm{e}}} \\ 0 & 0 & 0 \end{bmatrix} \tag{10b}$$

$$\boldsymbol{B}_{\mathrm{C}} = \begin{bmatrix} -1 & 0 \\ 0 & 0 \\ 0 & -1 \end{bmatrix}. \tag{10c}$$

For the control design purpose, the reference vector $\boldsymbol{r}_{\mathrm{C}}$ will not be taken into account, only $\boldsymbol{A}_{\mathrm{C}}$ and $\boldsymbol{B}_{\mathrm{C}}$. This vector will be added directly to the control law.

3.2 Dynamic LPV modelling

The dynamic model is quite more complex than the presented kinematic one. Thus, the development of an LPV model is more involved, and therefore it is presented in progressive steps.

Denoting the state, control and output vectors, respectively, as

$$\boldsymbol{x} = \begin{bmatrix} v \\ \alpha \\ \omega \end{bmatrix} \quad \boldsymbol{u}_{\mathrm{D}} = \begin{bmatrix} F_{x\mathrm{R}} \\ \delta \end{bmatrix} \tag{11}$$

and considering an unknown friction force disturbance as a variation of the nominal F_{friction} denoted as F_{fr}, the state-space model for the dynamic representation (2) can be obtained as

$$\dot{\boldsymbol{x}} = \boldsymbol{A}(\delta, v, \alpha)\boldsymbol{x} + \boldsymbol{B}(\delta, v, \alpha)\boldsymbol{u}_{\mathrm{D}} + \boldsymbol{E}F_{\mathrm{fr}} \tag{12a}$$

where

$$\boldsymbol{A}(\delta, v, \alpha) = \begin{bmatrix} A_{11} & A_{12} & A_{13} \\ 0 & A_{22} & A_{23} \\ 0 & A_{32} & A_{33} \end{bmatrix} \tag{12b}$$

$$A_{11} = -\frac{F_{df}}{Mv} \tag{12c}$$

$$A_{12} = \frac{C_x(\sin(\delta)\cos(\alpha) - \sin(\alpha)\cos(\delta) - \sin(\alpha))}{M} \tag{12d}$$

$$A_{13} = \frac{C_x(a(\sin(\delta)\cos(\alpha) - \sin(\alpha)\cos(\delta)) + b\sin(\alpha))}{Mv} \tag{12e}$$

$$A_{22} = \frac{-C_x(\cos(\alpha)\cos(\delta) + \sin(\alpha)\sin(\delta) + \cos(\alpha))}{Mv} \tag{12f}$$

$$A_{23} = \frac{-C_x a(\cos(\delta)\cos(\alpha) + \sin(\alpha)\sin(\delta)) + C_x b\cos(\alpha)}{Mv^2} - 1 \tag{12g}$$

$$A_{32} = \frac{C_x(b - a\cos(\delta))}{I} \quad A_{33} = \frac{-C_x(b^2 + a^2\cos(\delta))}{Iv} \tag{12h}$$

$$\boldsymbol{B}(\delta, v, \alpha) = \begin{bmatrix} B_{11} & B_{12} \\ B_{21} & B_{22} \\ 0 & B_{32} \end{bmatrix} \tag{12i}$$

$$B_{11} = \frac{\cos(\alpha)}{M} \quad B_{12} = \frac{C_x(-\sin(\delta)\cos(\alpha) + sin(\alpha)\cos(\delta))}{M} \tag{12j}$$

$$B_{21} = \frac{-\sin(\alpha)}{Mv} \quad B_{22} = \frac{C_x(\cos(\alpha)\cos(\delta) + \sin(\alpha)\sin(\delta))}{Mv} \tag{12k}$$

$$B_{32} = \frac{C_x a\cos(\delta)}{I} \tag{12l}$$

$$\boldsymbol{E} = \begin{bmatrix} \dfrac{-1}{M} \\ 0 \\ 0 \end{bmatrix}. \tag{12m}$$

At this point, $\boldsymbol{A}$ and $\boldsymbol{B}$ are time-varying matrices. However, with the aim of avoiding the dependency on varying parameters in matrix $\boldsymbol{B}$, the system has been augmented by adding a fast dynamic filter as suggested by Apkarin *et al.* [31] in the form

$$\dot{\boldsymbol{x}}_{\mathrm{f}} = \boldsymbol{A}_{\mathrm{f}}\boldsymbol{x}_{\mathrm{f}} + \boldsymbol{B}_{\mathrm{f}}\boldsymbol{u}_{\mathrm{f}} \tag{13}$$

$$\begin{bmatrix} \dot{F}_{x\mathrm{R}} \\ \dot{\delta} \end{bmatrix} = \begin{bmatrix} -\psi & 0 \\ 0 & -\psi \end{bmatrix}\begin{bmatrix} F_{x\mathrm{R}} \\ \delta \end{bmatrix} + \begin{bmatrix} \psi & 0 \\ 0 & \psi \end{bmatrix}\begin{bmatrix} u_{\mathrm{F}} \\ u_{\delta} \end{bmatrix}$$

where ψ represents the filter gain, u_{F} is the new longitudinal behaviour input and u_{δ} is the new lateral behaviour input. Note that these new added states have fast dynamics and will not disturb the dynamic model (12).

Then, the system (12) is transformed into a new fifth-order system with state and input vectors as

$$\tilde{\boldsymbol{x}} = \begin{bmatrix} v \\ \alpha \\ \omega \\ F_{x\mathrm{R}} \\ \delta \end{bmatrix} \quad \boldsymbol{u}_{\mathrm{f}} = \begin{bmatrix} u_{\mathrm{F}} \\ u_{\delta} \end{bmatrix} \tag{14a}$$

and matrices $\tilde{\boldsymbol{A}}$, $\tilde{\boldsymbol{B}}$ and $\tilde{\boldsymbol{E}}$ as

$$\tilde{\boldsymbol{A}}(\delta, v, \alpha) = \begin{bmatrix} A_{11} & A_{12} & A_{13} & B_{11} & B_{12} \\ 0 & A_{22} & A_{23} & B_{21} & B_{22} \\ 0 & A_{32} & A_{33} & 0 & B_{32} \\ 0 & 0 & 0 & -\psi & 0 \\ 0 & 0 & 0 & 0 & -\psi \end{bmatrix} \tag{14b}$$

$$\tilde{\boldsymbol{B}} = \begin{bmatrix} 0 & 0 \\ 0 & 0 \\ 0 & 0 \\ \psi & 0 \\ 0 & \psi \end{bmatrix} \quad \tilde{\boldsymbol{E}} = \begin{bmatrix} \dfrac{1}{M} \\ 0 \\ 0 \\ 0 \\ 0 \end{bmatrix}. \tag{14c}$$

However, the model still presents some features that will be difficult to control design task. One of them is that the input $\delta = 0$ has been identified as a singular point. Hence, to avoid it, a change of variable has been done by shifting the δ interval

$$\delta \in \left[\underline{\delta}, \overline{\delta}\right] \rightarrow \sigma \in \left[\underline{\delta} + \varepsilon, \overline{\delta} + \varepsilon\right] \tag{15}$$

converting σ into the new scheduling variable and being ε a constant value greater than $\overline{\delta}$.

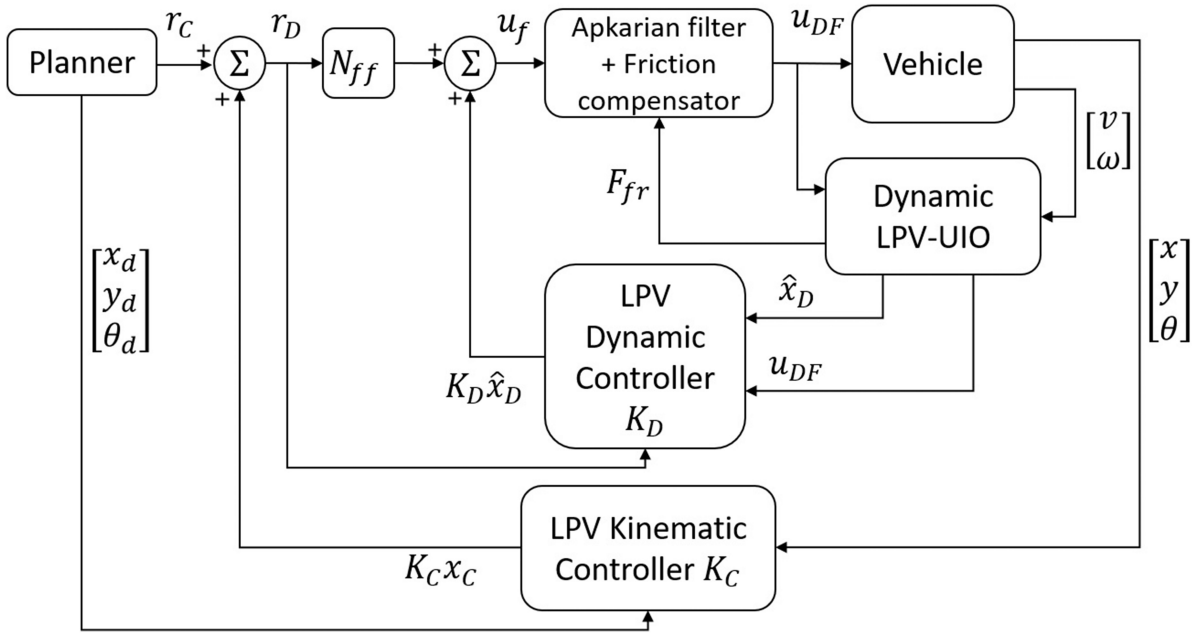

Fig. 2 *Complete autonomous driving control scheme with two LPV controllers and an LPV–UIO with friction force compensator. Note that both* $\boldsymbol{K}_D$ *and* $\boldsymbol{K}_C$ *have the negative sign embedded*

In addition to all these arrangements, it was found that the angular velocity channel lacks integral action, thus leading to a steady-state error. Hence, the addition of such action through the controller is considered. Then, a new state (i_p) has been added as the integral of the state ω

$$\dot{i}_p = -\omega\,. \tag{16}$$

Therefore, starting from (14), taking into account these considerations and denoting the scheduling variables as $\sigma, v, \alpha \in \mathbb{R}$, the vehicle dynamic LPV model can be expressed as follows:

$$\dot{\boldsymbol{x}}_{\mathrm{D}} = \boldsymbol{A}_{\mathrm{D}}(\sigma, v, \alpha)\boldsymbol{x}_{\mathrm{D}} + \boldsymbol{B}_{\mathrm{D}}\boldsymbol{u}_{\mathrm{f}} + \boldsymbol{E}_{\mathrm{D}}F_{\mathrm{fr}} \tag{17a}$$

with state and input vectors

$$\boldsymbol{x}_{\mathrm{D}} = \begin{bmatrix} v \\ \alpha \\ \omega \\ F_{x\mathrm{R}} \\ \sigma \\ i_p \end{bmatrix} \quad \boldsymbol{u}_{\mathrm{f}} = \begin{bmatrix} u_{\mathrm{F}} \\ u_{\delta} \end{bmatrix} \tag{17b}$$

and matrices $\boldsymbol{A}_{\mathrm{D}}$, $\boldsymbol{B}_{\mathrm{D}}$ and $\boldsymbol{E}_{\mathrm{D}}$ as

$$\boldsymbol{A}_{\mathrm{D}}(\sigma, v, \alpha) = \begin{bmatrix} A_{11} & A_{12} & A_{13} & B_{11} & B_{12} & 0 \\ 0 & A_{22} & A_{23} & B_{21} & B_{22} & 0 \\ 0 & A_{32} & A_{33} & 0 & B_{32} & 0 \\ 0 & 0 & 0 & -\psi & 0 & 0 \\ 0 & 0 & 0 & 0 & -\psi & 0 \\ 0 & 0 & -1 & 0 & 0 & 0 \end{bmatrix} \tag{17c}$$

$$\boldsymbol{B}_{\mathrm{D}} = \begin{bmatrix} 0 & 0 \\ 0 & 0 \\ 0 & 0 \\ \psi & 0 \\ 0 & \psi \\ 0 & 0 \end{bmatrix} \quad \boldsymbol{E}_{\mathrm{D}} = \begin{bmatrix} \frac{-1}{M} \\ 0 \\ 0 \\ 0 \\ 0 \\ 0 \end{bmatrix}. \tag{17d}$$

The model (17) will be used for designing the dynamic state feedback control. Hereafter, in order to simplify the notation, the scheduling variables dependency of state-space matrices is omitted.

4 LPV–UIO design

Owing to the lack of available sensors for measuring all states, i.e.: there is no one that measures the slip angle, the design of a state estimator has been considered in this section (see Fig. 2). The LPV–UIO tackles the problem of estimating both the dynamic states and the friction force affecting the vehicle. Such an estimator has been designed following an optimal approach exploiting the duality between the LQR and Kalman filter approaches. In a recent work [32], Pletschen and Diepold present a T–S Kalman filter strategy with a decoupled stability and performance methodology. Unlike that approach, this paper presents an LPV Kalman filter with both stability and performance criteria integrated in single design procedure.

4.1 System description

The proposed UIO estimation scheme is developed for LPV systems affected by external disturbances. The measurement model for the dynamical one presented in (12) considering the available sensors leads to consider the following output matrix:

$$\boldsymbol{C} = \begin{bmatrix} 1 & 0 & 0 \\ 0 & 0 & 1 \end{bmatrix} \tag{18}$$

due to the lack of measuring of dynamic states as the slip angle and the estimated vector state is denoted as

$$\hat{\boldsymbol{x}}_{\mathrm{DO}} = \begin{bmatrix} \hat{v} \\ \hat{\alpha} \\ \hat{\omega} \end{bmatrix}. \tag{19}$$

The proposed disturbance estimation is based on the UIO approach. Such a procedure is based on computing the difference between the real system and the model used for observation

$$\boldsymbol{CE}\mathrm{F}_{\mathrm{fr}} = \dot{\boldsymbol{y}} - \boldsymbol{C}(\boldsymbol{A}\hat{\boldsymbol{x}}_{\mathrm{DO}} + \boldsymbol{B}\boldsymbol{u})\,. \tag{20}$$

Thus, considering $\boldsymbol{\Theta} = (\boldsymbol{CE})^{+}$, the force friction disturbance can be obtained as

$$F_{\text{fr}} = \boldsymbol{\Theta}\left(\dot{\boldsymbol{y}} - \boldsymbol{C}(\boldsymbol{A}\hat{\boldsymbol{x}}_{\text{DO}} + \boldsymbol{B}\boldsymbol{u})\right). \tag{21}$$

Moreover consequently, decoupling the considered disturbance, the system (12) can be rewritten as follows:

$$\dot{\hat{\boldsymbol{x}}}_{\text{DO}} = \boldsymbol{A}_o\hat{\boldsymbol{x}}_{\text{DO}} + \boldsymbol{B}_o\boldsymbol{u} - \boldsymbol{E}\boldsymbol{\Theta}\dot{y} \tag{22}$$

where

$$\boldsymbol{A}_{\text{o}} = (\boldsymbol{I} - \boldsymbol{E}\boldsymbol{\Theta}\boldsymbol{C})\boldsymbol{A}$$
$$\boldsymbol{B}_{\text{o}} = (\boldsymbol{I} - \boldsymbol{E}\boldsymbol{\Theta}\boldsymbol{C})\boldsymbol{B}.$$

Then, the state estimation will depend on the observer gain $\boldsymbol{L}$ and presents the form

$$\dot{\hat{\boldsymbol{x}}}_{DO} = (\boldsymbol{A}_{\text{o}} - \boldsymbol{L}\boldsymbol{C})\hat{\boldsymbol{x}}_{\text{DO}} + \boldsymbol{B}_{\text{o}}\boldsymbol{u} - \boldsymbol{E}\boldsymbol{\Theta}\dot{\boldsymbol{y}} + \boldsymbol{L}\boldsymbol{y}. \tag{23}$$

4.2 Description of the design method

To design the observer gain $\boldsymbol{L}$ in (23), a polytopic approximation of (12) is used

$$\boldsymbol{A}(\boldsymbol{\Phi}) = \sum_{i=1}^{2^{n_\Phi}} \mu_i(\boldsymbol{\Phi})\boldsymbol{A}_i \tag{24}$$

where $\boldsymbol{A}_i$ are obtained using the bounding box approach, n_Φ is the number of scheduling variables, $\boldsymbol{\Phi}$ is the vector containing the scheduling variables defined as $\boldsymbol{\Phi} := \left[\vartheta_1(t), \ldots, \vartheta_{n_\Phi}(t)\right]$ and $\mu_i(\boldsymbol{\Phi})$ is given by

$$\mu_i(\boldsymbol{\Phi}) = \prod_{j=1}^{n_\Phi} \xi_{ij}(\eta_0^j, \eta_1^j) \quad i = \{1, \ldots, 2^{n_\Phi}\} \tag{25}$$

$$\begin{aligned} \eta_0^j &= \frac{\overline{\vartheta_j} - \vartheta_j(t)}{\overline{\vartheta_j} - \underline{\vartheta_j}} \\ \eta_1^j &= 1 - \eta_0^j \quad j = \{1, \ldots, n_\Phi\} \end{aligned} \tag{26}$$

where each variable ϑ_j is known and varies in a defined interval $\vartheta_j(t) \in \left[\underline{\vartheta_j}, \overline{\vartheta_j}\right]$.

Then, the observer gain is given by

$$\boldsymbol{L}(\boldsymbol{\Phi}) = \sum_{i=1}^{2^{n_\Phi}} \mu_i(\boldsymbol{\Phi})\boldsymbol{L}_i \tag{27}$$

where $\boldsymbol{L}_i$ are obtained using the following proposition that provides an optimal design based on the Riccati equations of the Kalman filter.

Proposition 1: Let the observer tuning parameters $\boldsymbol{Q} = \boldsymbol{Q}^{\text{T}} \geq 0$, $\boldsymbol{R} = \boldsymbol{R}^{\text{T}} > 0$, the optimal performance bound $\gamma > 0$, the decay rate $\lambda > 0$, the output matrix $\boldsymbol{C}$ in (18) and the matrices $\boldsymbol{A}_i$ in (24). Then, the polytopic observer gains in (27) are obtained by finding $\boldsymbol{Y}$ and $\boldsymbol{W}_i$ satisfying the following LMIs:

$$\begin{aligned} &\begin{bmatrix} \boldsymbol{Y}\boldsymbol{A}_i + \boldsymbol{A}_i{}^{\text{T}}\boldsymbol{Y} - \boldsymbol{W}_i\boldsymbol{C} - \boldsymbol{C}^{\text{T}}\boldsymbol{W}_i^{\text{T}} + \boldsymbol{Y}2\lambda & \boldsymbol{Y}(\boldsymbol{Q}^{1/2})^{\text{T}} & \boldsymbol{W}_i \\ \boldsymbol{Q}^{1/2}\boldsymbol{Y} & -\boldsymbol{I} & 0 \\ \boldsymbol{W}_i^{\text{T}} & 0 & -\boldsymbol{R}^{-1} \end{bmatrix} < 0 \\ &\begin{bmatrix} \gamma\boldsymbol{I} & \boldsymbol{I} \\ \boldsymbol{I} & \boldsymbol{Y} \end{bmatrix} > 0 \quad i = 1, \ldots, 2^{n_{Sv}} \end{aligned} \tag{28}$$

considering $\boldsymbol{Y} = \boldsymbol{Y}^{\text{T}} > 0$ and applying the transformation $\boldsymbol{L}_i = \boldsymbol{Y}^{-1}\boldsymbol{W}_i$.

Proof: Considering the Kalman filter Ricatti equation for every vertex of the polytopic model (24), the following inequality is obtained:

$$\dot{\boldsymbol{P}} = (\boldsymbol{A}_i - \boldsymbol{L}_i\boldsymbol{C})\boldsymbol{P} + \boldsymbol{P}(\boldsymbol{A}_i - \boldsymbol{L}_i\boldsymbol{C})^{\text{T}} + \boldsymbol{Q} + \boldsymbol{L}_i\boldsymbol{R}\boldsymbol{L}_i^{\text{T}} < 0.$$

At this point, we introduce an extra performance term, i.e. the decay rate (λ), for ensuring a fast dynamic response of the observer

$$(\boldsymbol{A}_i - \boldsymbol{L}_i\boldsymbol{C})\boldsymbol{P} + \boldsymbol{P}(\boldsymbol{A}_i - \boldsymbol{L}_i\boldsymbol{C})^{\text{T}} + 2\lambda\boldsymbol{P} + \boldsymbol{Q} + \boldsymbol{L}_i\boldsymbol{R}\boldsymbol{L}_i^{\text{T}} < 0.$$

Then, by multiplying first each term of the last inequality by $\boldsymbol{Y} = \boldsymbol{P}^{-1}$ from the left-hand and the right-hand sides and then by introducing $\boldsymbol{W}_i = \boldsymbol{Y}\boldsymbol{L}_i$, the following inequality is obtained:

$$\boldsymbol{Y}\boldsymbol{A}_i - \boldsymbol{W}_i\boldsymbol{C} + \boldsymbol{A}_i^{\text{T}} - \boldsymbol{C}^{\text{T}}\boldsymbol{W}_i^{\text{T}} + \boldsymbol{Y}2\lambda + \boldsymbol{Y}\boldsymbol{Q}\boldsymbol{Y} + \boldsymbol{W}_i\boldsymbol{R}\boldsymbol{W}_i^{\text{T}} < 0.$$

From here, we reformulate the inequality in order to use the Schur complement

$$\boldsymbol{Y}\boldsymbol{A}_i + \boldsymbol{A}_i^{\text{T}}\boldsymbol{Y} - \boldsymbol{W}_i\boldsymbol{C} - \boldsymbol{C}^{\text{T}}\boldsymbol{W}_i^{\text{T}} + \boldsymbol{Y}2\lambda$$

$$-\begin{bmatrix} \boldsymbol{Y}(\boldsymbol{Q}^{1/2})^{\text{T}} & \boldsymbol{W}_i \end{bmatrix}\begin{bmatrix} -I & 0 \\ 0 & -R \end{bmatrix}\begin{bmatrix} \boldsymbol{Q}^{1/2}\boldsymbol{Y} \\ \boldsymbol{W}_i^{\text{T}} \end{bmatrix} < 0.$$

Applying such a complement to this inequality the first LMI of (28) is obtained.

The second LMI starts by bounding the Lyapunov matrix

$$\boldsymbol{P} < \gamma\boldsymbol{I}.$$

Applying first the change of variable $\boldsymbol{Y} = \boldsymbol{P}^{-1}$ and then the Schur complement

$$\gamma\boldsymbol{I} - \boldsymbol{I}\boldsymbol{Y}^{-1}\boldsymbol{I} > 0$$

$$\begin{bmatrix} \gamma\boldsymbol{I} & \boldsymbol{I} \\ \boldsymbol{I} & \boldsymbol{Y} \end{bmatrix} > 0.$$

where the condition $\boldsymbol{P} > 0$ is included. □

Note that the problem has solution if and only if there exist $\boldsymbol{Y} \in \mathbb{R}^s$ and $\boldsymbol{W}_i \in \mathbb{R}^{s \times m}$, being s the number of states and m the number of measurable states. Matrices $\boldsymbol{Q}$ and $\boldsymbol{R}$ represent the process noise covariance and the sensor noise covariance, respectively.

4.3 Dynamic LPV–UIO design

The dynamic LPV–UIO tackles the problem of estimating the dynamic state vector in (19) as well as estimating the friction force acting over the vehicle.

At this point, the LPV model developed in (12) is used for solving the Proposition 1 using the output matrix (18). The chosen scheduling variables are σ, v and α bounded in the following intervals:

$$\sigma \in [5, 55]^{\circ} \text{ and } v \in [1, 18]\,\frac{m}{s}$$

$$\alpha \in [-0.1, 0.1]\,rad.$$

The proposed design matrices and parameters are: $\boldsymbol{R} = 0.01I_{2\times 2}$, $\boldsymbol{Q} = 0.01I_{3\times 3}$, $\gamma = 0.1$ and $\lambda = 12$. The solution of such a Proposition 1 returns the polytopic observer gains. Then, at every time step, the interpolated observer gain is obtained by means of (27).

Table 3 RMSE obtained for three different configurations of the LQR controllers

RMSE			Kinematic control design		Dynamic control design	
V	ω	Y	$\boldsymbol{Q}$	$\boldsymbol{R}$	$\boldsymbol{Q}$	$\boldsymbol{R}$
0.121	0.035	0.0177	[1, 1, 1]	[0.004, 0.0001]	[0.01, 0.01, 0.01, 0.01, 10, 3000]	[0.005, 0.6]
0.124	0.031	0.0196	[3, 5, 15]	[0.04, 0.01]	[0.01, 0.01, 0.01, 0.01, 100, 30000]	[0.005, 0.6]
0.076	0.0127	0.0213	[10, 3, 15]	[0.4, 0.001]	[0.01, 0.01, 0.01, 0.01, 1000, 90000]	[0.005, 0.6]
0.045	**0**.0077	**0**.05	[3, 2, 20]	[0.5, 0.001]	[0.01, 0.01, 0.01, 0.01, 100000, 90000]	[0.01, 10]

Values of $\boldsymbol{Q}$ and $\boldsymbol{R}$ represent the diagonal values of each matrix. Bold raw is the configuration chosen for the performed simulation.

5 Control design using LPV approach

The automatic control strategy addresses the problem of generating an appropriate vehicle behaviour from a desired reference. In this work, two cascade feedback LPV controllers are proposed for controlling appropriately the behaviour of the vehicle (see Fig. 2). Furthermore, a trajectory planner [33] is used which is in charge of providing the correspondent position and velocities references to the kinematic controller.

In this approach, a cascade methodology is employed where the internal and fast loop corresponds to the dynamic control and the external one to the kinematic control. On one hand, the kinematic control ($\boldsymbol{K}_{\mathrm{C}}$ in Fig. 2) is in charge of computing smooth control actions (linear and angular velocities) such that the vehicle is capable of achieving the required speed, position and orientation at the next local way point. On the other hand, the dynamic control strategy ($\boldsymbol{K}_D$ in Fig. 2) allows the vehicle to follow the angular and linear velocity references provided by the kinematic control loop. To this aim, the dynamic control generates forces to the rear wheels and a steering angle signal for the front wheels.

5.1 Description of the design method

Note that the design overview has been developed for the case of the dynamic model in (17). However, the same procedure is used for designing the kinematic controller by just considering the kinematic model in (10).

To design the controller $\boldsymbol{K}_{\mathrm{D}}$, the polytopic approach of the system in (17) is used in the same way it was presented in (24). Then, using (25) and (26), the controller gain is obtained by means of

$$\boldsymbol{K}_{\mathrm{D}}(\boldsymbol{\Phi}) = \sum_{i=1}^{2^{n_\Phi}} \mu_i(\boldsymbol{\Phi})\boldsymbol{K}_{\mathrm{D}_i} \tag{29}$$

where $\boldsymbol{K}_{\mathrm{D}_i}$ are obtained using the following proposition, which presents an LMI-based formulation for solving the LPV–LQR problem.

Proposition 2: Given the LQR parameters $\boldsymbol{Q} = \boldsymbol{Q}^{\mathrm{T}} \geq 0$, $\boldsymbol{R} = \boldsymbol{R}^{\mathrm{T}} > 0$, the optimal performance bound $\gamma > 0$, the decay rate $\eta > 0$ and the matrices $\boldsymbol{A}_{\mathrm{D}_i}$ obtained using (24). Then, the polytopic control gains in (29) are obtained by finding $\boldsymbol{P}$ and $\boldsymbol{W}_i$ satisfying the following LMIs:

$$\begin{aligned} &\boldsymbol{A}_{\mathrm{D}_i}\boldsymbol{P} + \boldsymbol{P}\boldsymbol{A}_{\mathrm{D}_i} - (\boldsymbol{B}_{\mathrm{D}}\boldsymbol{W}_i)^{\mathrm{T}} - \boldsymbol{B}_{\mathrm{D}}\boldsymbol{W}_i + 2\eta\boldsymbol{P} < 0 \\ &\begin{bmatrix} \boldsymbol{W}_i^{\mathrm{T}}\boldsymbol{R}\boldsymbol{W}_i & \boldsymbol{P}(\boldsymbol{Q}^{1/2})^{T} \\ \boldsymbol{P} & (-\boldsymbol{Q}^{\frac{1}{2}})^{-1} \end{bmatrix} < 0 \quad i = 1, \ldots, 2^{n_\Phi} \\ &0 < \boldsymbol{P} < \gamma \end{aligned} \tag{30}$$

and applying the transformation $\boldsymbol{K}_{\mathrm{D}_i} = \boldsymbol{W}_i\boldsymbol{P}^{-1}$.

Proof: Considering the LQR Riccati equation for every vertex of the polytopic model (17), the following inequality is obtained:

$$(\boldsymbol{A}_i - \boldsymbol{B}_{\mathrm{D}}\boldsymbol{K}_{\mathrm{D}_i})^{\mathrm{T}}\boldsymbol{P} + \boldsymbol{P}(\boldsymbol{A}_i - \boldsymbol{B}_{\mathrm{D}}\boldsymbol{K}_{\mathrm{D}_i}) + \boldsymbol{Q} + \boldsymbol{K}_{\mathrm{D}_i}^{\mathrm{T}}\boldsymbol{R}\boldsymbol{K}_{\mathrm{D}_i} < 0\,.$$

At this point, we split the last inequality in two new ones. The first resultant is the pure Lyapunov stability term

$$(\boldsymbol{A}_{\mathrm{D}_i} - \boldsymbol{B}_{\mathrm{D}}\boldsymbol{K}_{\mathrm{D}_i})^{\mathrm{T}}\boldsymbol{P} + \boldsymbol{P}(\boldsymbol{A}_{\mathrm{D}_i} - \boldsymbol{B}_{\mathrm{D}}\boldsymbol{K}_{\mathrm{D}_i}) < 0$$

where, to ensure a fast dynamic response of the controller, a decay rate term (η) has been added obtaining

$$(\boldsymbol{A}_{\mathrm{D}_i} - \boldsymbol{B}_{\mathrm{D}}\boldsymbol{K}_{\mathrm{D}_i})^{\mathrm{T}}\boldsymbol{P} + \boldsymbol{P}(\boldsymbol{A}_{\mathrm{D}_i} - \boldsymbol{B}_{\mathrm{D}}\boldsymbol{K}_{\mathrm{D}_i}) + 2\eta\boldsymbol{P} < 0$$

and applying $\boldsymbol{K}_{D_i} = \boldsymbol{W}_i\boldsymbol{P}^{-1}$ we obtain the following LMI:

$$\boldsymbol{A}_{D_i}\boldsymbol{P} + \boldsymbol{P}\boldsymbol{A}_{D_i} - (\boldsymbol{B}_D\boldsymbol{W}_i)^{\mathrm{T}} - \boldsymbol{B}_D\boldsymbol{W}_i + 2\eta\boldsymbol{P} < 0\,.$$

The second LMI establishes the LQR performance. Then, multiplying by the left-hand and right-hand second part of the Riccati equation we achieve

$$\boldsymbol{P}(\boldsymbol{Q}^{1/2})^{\mathrm{T}}\boldsymbol{Q}^{1/2}\boldsymbol{P} + \boldsymbol{P}\boldsymbol{K}_{\mathrm{D}_i}^{\mathrm{T}}\boldsymbol{R}\boldsymbol{K}_{\mathrm{D}_i}\boldsymbol{P} < 0$$

and applying the change $\boldsymbol{K}_{\mathrm{D}_i} = \boldsymbol{W}_i\boldsymbol{P}^{-1}$ it is converted to

$$\boldsymbol{P}(\boldsymbol{Q}^{1/2})^{\mathrm{T}}\boldsymbol{Q}^{1/2}\boldsymbol{P} + \boldsymbol{W}_i^{\mathrm{T}}\boldsymbol{R}\boldsymbol{W}_i < 0.$$

At this point, by rearranging the elements we obtain

$$\boldsymbol{W}_i^{\mathrm{T}}\boldsymbol{R}\boldsymbol{W}_i - \boldsymbol{P}(\boldsymbol{Q}^{1/2})^{\mathrm{T}}(-\boldsymbol{Q}^{1/2})\boldsymbol{P} < 0$$

and using the Schur complement, the resulting LMI is as follows:

$$\begin{bmatrix} \boldsymbol{W}_i^{\mathrm{T}}\boldsymbol{R}\boldsymbol{W}_i & \boldsymbol{P}(\boldsymbol{Q}^{1/2})^{\mathrm{T}} \\ \boldsymbol{P} & (-\boldsymbol{Q}^{1/2})^{-1} \end{bmatrix} < 0.$$

□

Note that the problem has solution if and only if there exist $\boldsymbol{P} \in \mathbb{R}^{\mathrm{s}}$, $\boldsymbol{H} \in \mathbb{R}^{\mathrm{r}}$ and $\boldsymbol{W}_i \in \mathbb{R}^{\mathrm{r}\times\mathrm{s}}$, being r the number of control actions and s the number of states. Observe also that decreasing the parameter γ increases the performance of the control loop.

Next sections provide details of the particular control design for the dynamic and kinematic vehicle controllers.

5.2 Dynamic LPV control design

The dynamic control addresses the tracking of the linear and angular velocity references of the vehicle by applying force to the wheels and an angle to the front wheels.

At this point, the LPV model developed in Section 3.2 is used for solving the Proposition 2. The chosen scheduling variables are σ, v and α which are bounded in the same intervals than the ones presented in Section 4.3.

The proposed design matrices $\boldsymbol{Q}$ and $\boldsymbol{R}$ are presented in Table 3. Parameters γ and η are set as 0.001 and 3, respectively. Looking for a solution for the Proposition 2, this returns the polytopic control gains $\boldsymbol{K}_{\mathrm{D}_i}$. Then, the controller obtained at each control iteration follows the rule presented in (29).

The proposed control scheme for this dynamic loop is a state feedback plus feedforward control. The function of feedforward

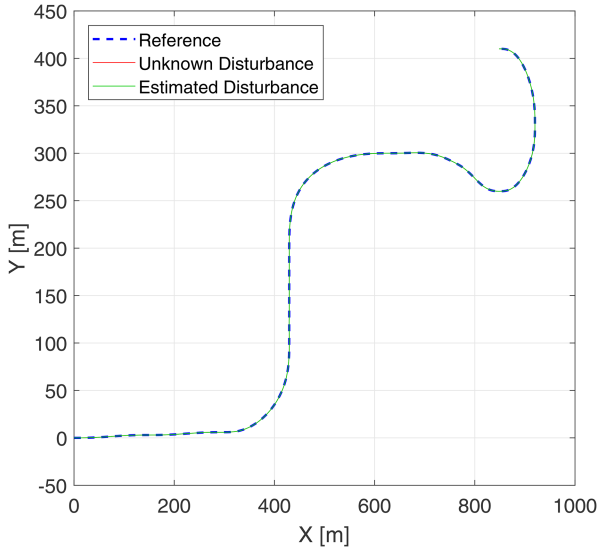

Fig. 3 *Proposed circuit for simulation and the result of solving the mixed control problem*

matrix is to make the gain of the system unitary. Such a matrix is computed following the next expression:

$$\boldsymbol{N}_{\mathrm{ff}} = \left[\tilde{\boldsymbol{C}}\left(-\tilde{\boldsymbol{B}}\boldsymbol{K} - \tilde{\boldsymbol{A}}\right)^{-1}\tilde{\boldsymbol{B}}\right]^{-1} \tag{31}$$

where matrices $\tilde{\boldsymbol{A}}$ and $\tilde{\boldsymbol{B}}$ are the ones presented in (14), $\boldsymbol{K}$ is a sub-block of $\boldsymbol{K}_D$, in which the last column has been omitted as it is proposed in [34]. Matrix $\tilde{\boldsymbol{C}}$ is of the form

$$\tilde{\boldsymbol{C}} = \begin{bmatrix} 1 & 0 & 0 & 0 & 0 \\ 0 & 0 & 1 & 0 & 0 \end{bmatrix}. \tag{32}$$

Therefore, the complete control law is expressed as

$$\boldsymbol{u}_{\mathrm{f}} = \boldsymbol{K}_{\mathrm{D}}\left[\hat{\boldsymbol{x}}_{\mathrm{DO}}\, F_{x\mathrm{R}}\, \sigma\, i_p\right]^{\mathrm{T}} + \boldsymbol{N}_{\mathrm{ff}}\boldsymbol{r}_{\mathrm{D}} \tag{33}$$

where the state vector is the one presented in (17b) though with the estimated dynamic states shown in (19), $\boldsymbol{r}_{\mathrm{D}}$ represents the reference vector which corresponds to the kinematic control signal $\boldsymbol{u}_{\mathrm{C}}$ and $\boldsymbol{u}_{\mathrm{f}}$ is the control input to the Apkarian filter added (13).

At this point, the dynamic control action $\boldsymbol{u}_{\mathrm{DF}}$ (see Fig. 2) is computed as the sum of the Apkarian filter result ($\boldsymbol{x}_{\mathrm{f}}$) and the vector generated by the friction force compensator in (21)

$$\boldsymbol{u}_{DF} = \begin{bmatrix} F_{xR} \\ \delta \end{bmatrix} + \begin{bmatrix} F_{fr} \\ 0 \end{bmatrix}. \tag{34}$$

It is interesting to note that, for controlling the vehicle in the interval $v_{\mathrm{d}} \in [0, 1]$ a translation has been applied. Thus, this means that when computing the controller at $v_d = 0(m/s)$, we are actually computing the controller at $v_{\mathrm{d}} = 1(m/s)$ and using it as we were in $v_{\mathrm{d}} = 0(m/s)$. In this way, we avoid to develop a hybrid control for this reduced velocity interval.

5.3 Kinematic LPV control design

Kinematic control is in charge of controlling the position, orientation and linear velocity by means of actuating over the linear and angular velocities of the vehicle.

At this moment, the kinematic LPV model (10) is employed for solving the Proposition 2. Three scheduling variables (v_{d}, ω and θ_e) are bounded in the following intervals:

$$v_{\mathrm{d}} \in [1, 18]\,\frac{m}{s} \quad \omega \in [-1.417, 1.417]\,\frac{\mathrm{rad}}{\mathrm{s}}$$

$$\theta_{\mathrm{e}} \in [-8, 8]^{\circ}.$$

The control design matrices $\boldsymbol{Q}$ and $\boldsymbol{R}$ are presented in Table 3 and parameter γ is set as 0.01. The Proposition 2 returns for this kinematic case the control matrices $\boldsymbol{K}_{\mathrm{C}_i}$ for each one of the polytopic vertexes. Then, the controller obtained at each control iteration ($\boldsymbol{K}_{\mathrm{C}}$) follows the rule presented in (29).

It is important to remark that, in this kinematic case, the Proposition 2 has a different configuration with respect to the dynamic case. The first inequality of (30) is negative and an additional LMI has been added to the Proposition 2

$$\boldsymbol{A}_{\mathrm{D}_i}\boldsymbol{P} + \boldsymbol{P}\boldsymbol{A}_{\mathrm{D}_i} - (\boldsymbol{B}_{\mathrm{D}}\boldsymbol{W}_i)^{\mathrm{T}} - \boldsymbol{B}_{\mathrm{D}}\boldsymbol{W}_i + 2\beta\boldsymbol{P} < 0\,. \tag{35}$$

Being $\beta = 0$, the LMI establishes a threshold for ensuring only stability. Thus, in order to increase the kinematic loop performance β can be increasing while being always positive. Here, it has been set to 0.1.

The following state feedback control law has been used for controlling the kinematic behaviour loop:

$$\boldsymbol{u}_{\mathrm{C}} = \boldsymbol{K}_{\mathrm{C}}\boldsymbol{x}_{\mathrm{C}} + \boldsymbol{r}_{\mathrm{C}} \tag{36}$$

where $\boldsymbol{x}_{\mathrm{C}}$ and $\boldsymbol{r}_{\mathrm{C}}$ are the kinematic state and position reference vectors, respectively, presented in (9). Such a reference is provided by a trajectory planner (see Fig. 2).

6 Simulation results

The simulation scenario (see Fig. 3) chosen for testing the automatic control strategy tries to cover different driving situations as acceleration stages and velocity reduction on curves as well as driving on different road conditions, as, e.g. asphalt or ice.

To deal with this changing road conditions, the friction force compensation mechanism is used and compared its result with the case of unknown friction.

Considering this information (circuit shape and varying velocity), a trajectory planner is in charge of generating a feasible trajectory by means of using a polynomial curve generation method [33]. This consists of computing continuous and differentiable curves (velocities and accelerations) under an overall constrained vehicle acceleration. Thus, in an offline mode, this planner algorithm generates the linear and angular velocity references as well as desired positions and orientations for the outer control loop (i.e. the kinematic control).

The adjustment of the LPV–LQR parameters ($\boldsymbol{Q}$, $\boldsymbol{R}$ and γ) is made by means of using the root mean square error (RMSE) approach. This measure allows to find suitable control parameters by minimising it. Linear velocity, angular velocity and lateral error are chosen by an exhaustive search. Moreover, η and β have been selected with the aim of increasing the performance of the closed-loop system. Table 3 shows some RMSE results for different control adjustments and the one considered in the simulations. Note that the observer adjustment was presented in Section 4.3.

In the tuning process, we have observed that the vehicle lateral behaviour is more difficult to control due to the changing reference. Hence, for the dynamic control case, the weight in $\boldsymbol{Q}$ corresponding to the dynamic integral state has been set much bigger than the rest. The same occurs in matrix $\boldsymbol{R}$.

The sample times used in both control loops are 0.1 and 0.01 s for kinematic and dynamic loops, respectively. The control strategy jointly with the trajectory planner are tested in MATLAB environment.

Figs. 3–6 show the vehicle results with known and unknown friction disturbances in the simulated circuit. Fig. 7*a* depicts the applied disturbance profile, i.e. friction force profile depending on the type of road (asphalt and ice). Finally, Fig. 7*b* represents the location of the closed-loop poles of kinematic and dynamic controllers, and the thresholds for the decay rate (η and β) used in their design.

Fig. 3 depicts the trajectory proposed and the result of both known and unknown disturbance scenarios.

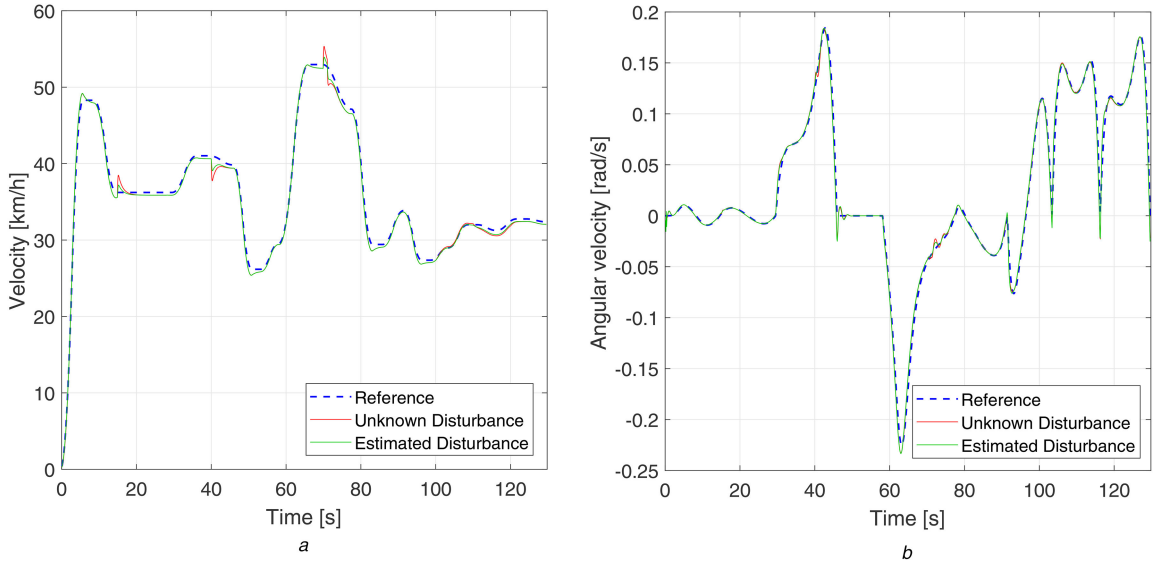

Fig. 4 *Velocities of the vehicle*
(a) Linear velocity reference and response, ***(b)*** Desired and simulated angular velocities

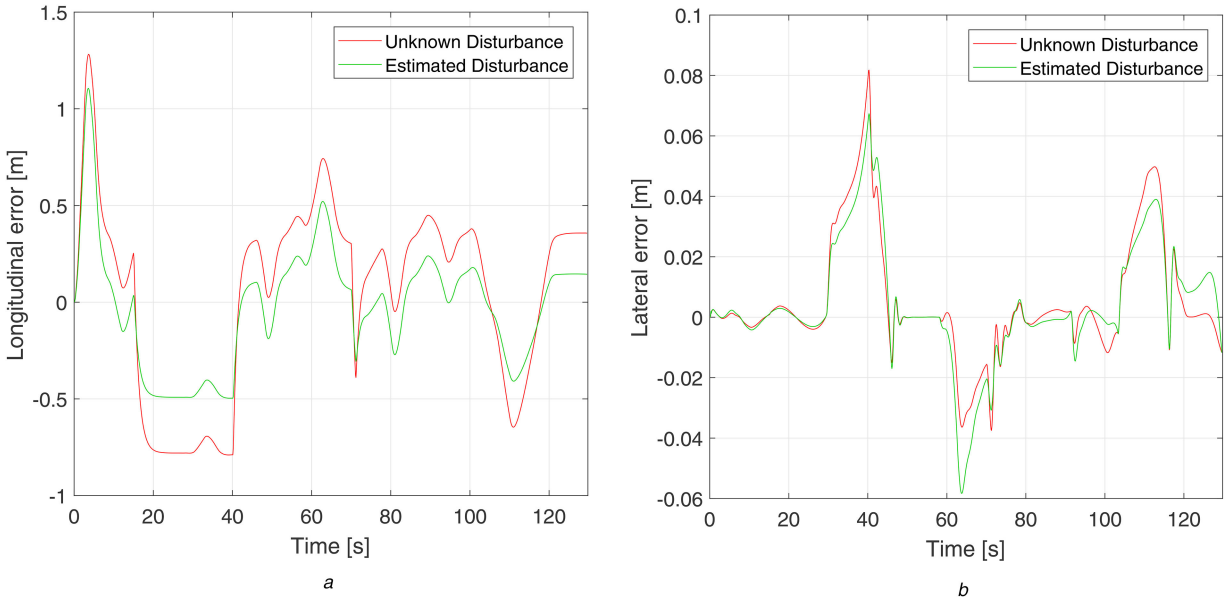

Fig. 5 *Resulting position errors*
(a) Vehicle longitudinal error along the circuit, ***(b)*** Vehicle lateral error

Fig. 4*a* shows the velocity response and that the friction force compensation mechanism works. In the case of unknown friction force, the controller is able to reject the disturbance. However, the estimation of the friction force by means of the UIO allows us to implement a compensation mechanism that makes the controller to reject the disturbance faster than in the case such estimation is not available. Fig. 4*b* depicts how the angular velocity performance is higher than the linear velocity one with respect to the reference. In addition, it can be appreciated how the compensation mechanism corrects also faster than in the case of unknown disturbance. Even so, the angular response presents some overshoot behaviour at some time instants. The controller adjustment may be one of the reasons, but the main reason is the high abruptness of the angular velocity reference at the end of the curves producing a rough behaviour on the vehicle.

Fig. 5 presents position errors for both cases. It can be seen the better performance when the disturbance is compensated. The mitigation of these errors is crucial for achieving a good autonomous guidance. However, a near-zero lateral error is more important since it ensures the driving of the vehicle through the centre of the road. In our results, longitudinal error is no longer than 0.5 m in normal driving (i.e. neither accelerating nor braking). Lateral error remains in the scale of few decimetres being increased when both velocities (angular and linear) increase. In addition to this graphical comparison, a quantitative one in terms of the RMSE has been performed (see Table 4). Such results verify the improvement of using the friction force compensation mechanism.

Fig. 6 shows the resulting control actions. The compensation mechanism allows to reduce the control effort being the action also smoother than in the unknown friction case. Note also that the steering angle signal in the first part of the simulation is quite abrupt. This behaviour is due to longitudinal and angular behaviours are highly coupled and the starting stage deals with high linear accelerations.

Fig. 7*a* shows the real friction force considered along the circuit simulated and the estimated force.

Fig. 7*b* illustrates the closed poles for the kinematic and dynamic loops at a given operating point. It can be observed that the poles of both loops satisfy the constraints imposed by the corresponding decay rates η and β [see (30) and (35)]. The satisfaction of this condition allows to design both loops separately, since the dynamic control presents a faster dynamic behaviour than the kinematic one.

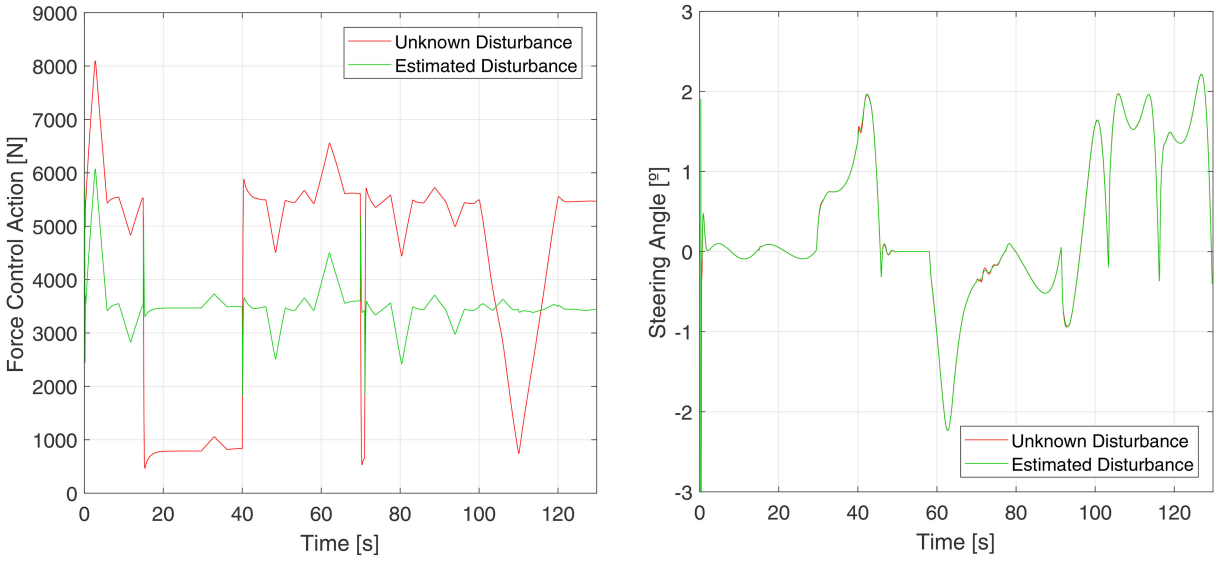

a *b*

Fig. 6 *Resulting control actions:*
(a) Force control action; ***(b)*** Steering angle

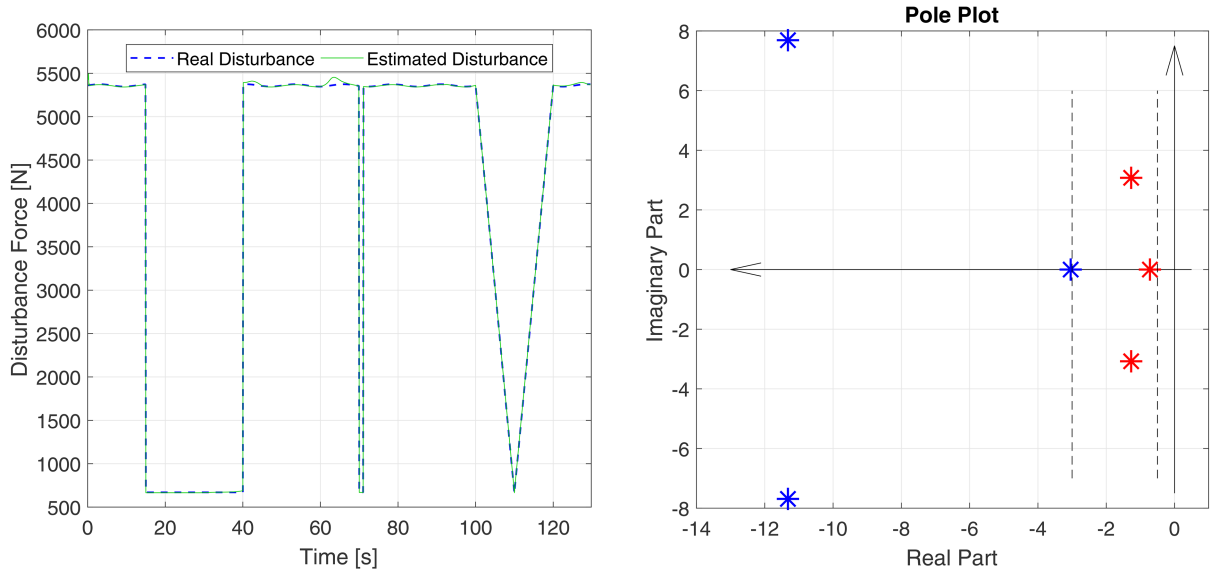

a *b*

Fig. 7 *Disturbance profile and system poles location.*
(a) Real and estimated disturbances, ***(b)*** Pole locus of the system in a particular operating point ($v = 8.33(m/s)$, $\omega = 0.05(rad/s)$ and $\alpha = 0.013$ rad). Blue marks are the three slower poles of the dynamic loop and the red ones are the kinematic poles. Vertical dashed lines represent the hyperplanes $\eta = 3$ and $\beta = 0.1$

Table 4 Comparison of both approaches using a quadratic measure and the maximum error values in metres

Approach	RMSE_v	RMSE_ω	RMSE_y	$x_{e_{\max}}$	$y_{e_{\max}}$
unknown	0.3834	0.0043	0.0204	1.2815	1.1055
estimated	0.2337	0.0041	0.0201	0.082	0.067

7 Conclusions

A gain-scheduling LPV–LQR control scheme has been introduced for solving the mixed control problem. To this aim, two models, i.e. kinematic and dynamic, have been expressed in the LPV form and an approach based on cascade design of the kinematic and dynamic controllers has been adopted with the aim of increasing the performance of the system. This is achieved by forcing the inner closed-loop dynamics to behave faster than the outer closed-loop one. Moreover, an UIO has been presented. It solves the problem of the lack of measurability in the case of the slip angle by estimating all the dynamic states as well as the friction force affecting the vehicle. Then, a friction force compensation mechanism is presented allowing the vehicle to compensate faster the disturbances caused by changes in the friction force as well as reducing the control effort.

Two novel LMI-based optimal designs for LPV observer and controller have been introduced.

They also present new integrated constraints for ensuring a certain level of control and observation performance.

The obtained gain-scheduling LPV–LQR control approach, jointly with the UIO and a trajectory planning module, has presented suitable results in a simulated scenario. In the same way, a comparison is shown about the friction force estimation, which shows the usefulness of this approach.

As a future work, this integrated control approach will be compared with other control strategies. Also, the proposed

modelling will be extended by adding steering dynamics and tyre slip situation. Finally, this controller–observer approach will be tested in a real scenario.

8 Acknowledgments

This work has been funded by the Spanish Ministry of Economy and Competitiveness (MINECO) and FEDER through the projects SCAV (ref. DPI2017-88403-R) and HARCRICS (ref. DPI2014-58104-R). The author is supported by a FI AGAUR grant (ref 2017 FI B00433).

9 References

[1] Van Woensel, L., Archer, G., Panades-Estruch, L., *et al.*: '*Ten technologies which could change our lives*' (European Union, Brussels, Belgium, 2015)

[2] 'United Nations, World Urbanization Prospects, United Nations, Department of Economic and Social Affairs, Population Division', 2014. Available at https://esa.un.org/unpd/wup/publications/files/wup2014-highlights.Pdf, Accessed date: 20/04/2018

[3] Warrendale, P.: 'Levels of automation for on-road vehicles, Society of Automotive Engineers (SAE)', 2014. Available at https://www.sae.org/misc/pdfs/automated_driving.pdf, Accessed date: 23/08/2017

[4] Paden, B., Čáp, M., Yong, S.Z., *et al.*: 'A survey of motion planning and control techniques for self-driving urban vehicles', *IEEE Trans. Intell. Veh.*, 2016, **1**, (1), pp. 33–55

[5] Chen, H., Guo, L., Qu, T., *et al.*: 'Optimal control methods in intelligent vehicles', *J. Control Decis.*, 2017, **4**, (1), pp. 32–56

[6] Polack, P., D'Andréa-Novel, B., Fliess, M., *et al.*: 'Finite-time stabilization of longitudinal control for autonomous vehicles via a model-free approach', *IFAC-PapersOnLine*, 2017, **50**, (1), pp. 12533–12538

[7] Fergani, S., Sename, O., Dugard, L.: 'An LPV/H_∞ integrated vehicle dynamic controller', *IEEE Trans. Veh. Technol.*, 2016, **65**, (4), pp. 1880–1889

[8] Alcala, E., Puig, V., Quevedo, J., *et al.*: 'Autonomous vehicle control using a kinematic Lyapunov-based technique with LQR-LMI tuning', *Control Eng. Pract.*, 2018, **73**, pp. 1–12

[9] Nawash, N.: 'H-infinity control of an autonomous mobile robot'. Master of science thesis, Cleveland State University, 2005

[10] Alcalá, E., Sellart, L., Puig, V., *et al.*: 'Comparison of two non-linear model-based control strategies for autonomous vehicles'. 2016 24th Mediterranean Conf. Control and Automation (MED), Athens (Greece), 2016, pp. 846–851

[11] Indiveri, G.: 'Kinematic time-invariant control of a 2D nonholonomic vehicle'. Proc. 38th IEEE Conf. Decision and Control, Phoenix, AZ, USA, 1999, vol. 3, pp. 2112–2117

[12] Blažič, S.: 'Takagi–Sugeno vs. Lyapunov-based tracking control for a wheeled mobile robot', *WSEAS Trans. Syst. Control*, 2010, **5**, (8), pp. 667–676

[13] Dixon, W.E., Dawson, D.M., Zergeroglu, E., *et al.*: '*Nonlinear control of wheeled mobile robots*' (Springer, London, 2000)

[14] Németh, B., Gáspár, P., Bokor, J.: 'LPV-based integrated vehicle control design considering the nonlinear characteristics of the tire'. American Control Conf. (ACC), 2016, Boston, 2016, pp. 6893–6898

[15] Gáspár, P., Szabó, Z., Bokor, J., *et al.*: '*Robust control design for active driver assistance systems*' (Springer, Switzerland, 2016), DOI: 10.1007/978-3-319-46126-7

[16] Olsson, C.: 'Model complexity and coupling of longitudinal and lateral control in autonomous vehicles using model predictive control', 2015

[17] González, R., Fiacchini, M., Guzmán, J.L., *et al.*: 'Robust tube-based predictive control for mobile robots in off-road conditions', *Robot. Auton. Syst.*, 2011, **59**, (10), pp. 711–726

[18] Nahidi, A., Kasaiezadeh, A., Khosravani, S., *et al.*: 'Modular integrated longitudinal and lateral vehicle stability control for electric vehicles', *Mechatronics*, 2017, **44**, pp. 60–70

[19] Farrokhsiar, M., Pavlik, G., Najjaran, H.: 'An integrated robust probing motion planning and control scheme: a tube-based MPC approach', *Robot. Auton. Syst.*, 2013, **61**, (12), pp. 1379–1391

[20] Schwarting, W., Alonso-Mora, J., Pauli, L., *et al.*: 'Parallel autonomy in automated vehicles: safe motion generation with minimal intervention'. 2017 IEEE Int. Conf. on Robotics and Automation (ICRA), Singapore, 2017, pp. 1928–1935

[21] Gao, Y., Gray, A., Tseng, H.E., *et al.*: 'A tube-based robust nonlinear predictive control approach to semi-autonomous ground vehicles', *Veh. Syst. Dyn., Int. J. Veh. Mech. Mob.*, 2014, **52**, (6), pp. 802–823

[22] Carvalho, A., Lefévre, S., Schildbach, G., *et al.*: 'Automated driving: the role of forecasts and uncertainty – a control perspective', *Eur. J. Control*, 2015, **24**, pp. 14–32

[23] Bascetta, L., Ferretti, G., Matteucci, M., *et al.*: 'LFT-based MPC control of an autonomous vehicle', *IFAC-PapersOnLine*, 2016, **49**, (15), pp. 7–12

[24] Rotondo, D.: '*Advances in gain-scheduling and fault tolerant control techniques*' (Springer, Barcelona, Spain, 2017)

[25] Ostertag, E.: '*Mono-and multivariable control and estimation: linear, quadratic and LMI methods*' (Springer Science & Business Media, Strasbourg, France, 2011)

[26] Duan, G.-R., Yu, H.-H.: '*LMIs in control systems: analysis, design and applications*' (CRC press, New York, USA, 2013)

[27] Yi, K., Hedrick, K., Lee, S.-C.: 'Estimation of tire-road friction using observer based identifiers', *Veh. Syst. Dyn.*, 1999, **31**, (4), pp. 233–261

[28] Svendenius, J.: 'Tire modeling and friction estimation'. PhD thesis, 2007

[29] Dakhlallah, J., Glaser, S., Mammar, S., *et al.*: 'Tire-road forces estimation using extended kalman filter and sideslip angle evaluation'. American Control Conf., 2008, Seattle, Washington, USA, 2008, pp. 4597–4602

[30] Rotondo, D., Cristofaro, A., Johansen, T.A., *et al.*: 'Diagnosis of icing and actuator faults in UAVs using LPV unknown input observers', *J. Intell. Robot. Syst.*, 2017, pp. 1–15

[31] Apkarian, P., Gahinet, P., Becker, G.: 'Self-scheduled H infinite control of linear parameter-varying systems: a design example', *Automatica*, 1995, **31**, (9), pp. 1251–1261

[32] Pletschen, N., Diepold, K.J.: 'Nonlinear state estimation for suspension control applications: a Takagi–Sugeno Kalman filtering approach', *Control Eng. Pract.*, 2017, **61**, pp. 292–306

[33] Bianco, C.G.L., Piazzi, A., Romano, M.: 'Velocity planning for autonomous vehicles'. IEEE Intelligent Vehicles Symp., Parma, Italy, 2004

[34] Franklin, G.F., Powell, J.D., Workman, M.L.: '*Digital control of dynamic systems*', vol. **3** (Addison-wesley, Menlo Park, CA, 1998)